



Semnan University



Free Vibration and Buckling Analyses of Functionally Graded Nanocomposite Plates Reinforced by Carbon Nanotube

R. Moradi-Dastjerdi ^{a*}, H. Malek-Mohammadi ^b

^a Young Researchers and Elite Club, Khomeinishahr Branch, Islamic Azad University, Khomeinishahr, Iran

^b Department of Mechanical Engineering, Bu-Ali Sina University, Hamedan, Iran

PAPER INFO

Paper history:

Received 2016-10-05

Revised 2016-11-18

Accepted 2016-11-19

Keywords:

Mori-Tanaka approach

Refined plate theory

Aggregated carbon nanotubes

Free vibration

Buckling

ABSTRACT

This paper describes the application of refined plate theory to investigate free vibration and buckling analyses of functionally graded nanocomposite plates reinforced by aggregated carbon nanotube (CNT). The refined shear deformation plate theory (RSDT) uses four independent unknowns and accounts for a quadratic variation of the transverse shear strains across the thickness, satisfying the zero traction boundary conditions on the top and bottom surfaces of the plate without using shear correction factors. The motion equations are derived from Hamilton's energy principle and Navier's method is applied to solve this equation. The material properties of the functionally graded carbon nanotube reinforced composites (FG-CNTRCs) are assumed to vary along the thickness and estimated with the Mori-Tanaka approach. Effects on the natural frequency and critical buckling load of the FG-CNTRC plates by CNT volume fraction, CNT distribution, CNT cluster distribution, and geometric dimensions of the plate are investigated. Effects of loading conditions on the critical buckling load are also examined.

DOI: 10.22075/MACS.2016.496

© 2017 Published by Semnan University Press. All rights reserved.

1. Introduction

Carbon nanotubes (CNTs), a new type of advanced material, have attracted a great deal of interest from researchers. Because of their extremely attractive mechanical, electrical and thermal properties, CNTs show promising application in polymer composites as a potential reinforcement and multifunctional element [1,2]. The introduction of CNTs into a polymer matrix may therefore greatly improve mechanical properties, such as tensile strength and elastic modulus, of the resulting nanocomposites [3]. Molecular dynamics (MD) is one technique that can be used to study CNTs. Han and Elliott [4] successfully used the MD method to determine the elastic modulus of composite structures under CNT reinforcement, and they investigated the effect of CNT volume fraction on mechanical properties of nanocomposites. They also investigated the effect of CNT waviness on the elastic properties and

mechanical behavior of carbon nanotube reinforced composites (CNTRCs). Alian et al. [5] used a multiscale modeling technique to determine the effective elastic moduli of nanocomposite reinforced by agglomerated carbon nanotubes. Their results showed that the effective elastic properties of the nanocomposite decreased by increasing in CNT volume that is located in CNT clusters. The significant effect of CNT waviness on the load transfer and active constrained layer damping behavior of the short fuzzy fiber-reinforced composite has been investigated [6-8]. Wuite and Adali [9] used a multiscale analysis to study the effects of volume, diameter and distribution of CNTs on deflection and static behavior of CNTRC beams. Formica et al. [10] presented the vibration behavior of CNTRC plates by employing an equivalent continuum model based on the Mori-Tanaka approach. They found that the improvement in modal properties achieved a maximum when the carbon nanotubes were uniformly

* Corresponding author. Tel.: +98-913-2058928, Fax: +98-31-33660088

E-mail address: rasoul.moradi@iaukhsh.ac.ir

aligned along the loading direction. Vodenitcharova and Zhang [11] used the Airy stress-function method to experimentally and computationally investigate pure bending and bending-induced local buckling of a nanocomposite beam reinforced by a single walled carbon nanotube (SWCNT).

Functionally graded materials (FGMs) are inhomogeneous composites characterized by smooth and continuous variations in both compositional profile and material properties. Such excellent qualities allow them to be fabricated as different structures in accordance with various service requirements. To obtain the required optimum performance, the gradient variation of material properties can be achieved by gradually changing the volume fraction of the constituent materials. Reddy [12] presented static and dynamic analyses of the FGM plates based on third order shear deformation theory and by using the theoretical formulation and finite element models. Zenkour [13] presented a two dimensional solution to study the bending, buckling, and free vibration of simply supported FG ceramic-metal sandwich plates. Cheng and Batra [14] used first and third order shear deformation theories to report deflections of a simply supported functionally graded polygonal plate. Also, Cheng and Batra [15] studied the buckling and steady state vibrations of a simply supported functionally graded polygonal plate based on Reddy's plate theory. Amabili et al. [16] compared Von Kármán, and first (FSDT) and third order shear deformation theories for non-linear vibration analysis of rectangular laminated composite plates with different boundary conditions, revealing that FSDT (with shear correction factor of $\sqrt{3}/2$) and the higher-order shear deformation theory give practically coincident results. Khorshidi et al. [17-18] analyzed vibration behaviour of laminated composite and functionally graded plates in contact with a bounded fluid using the Rayleigh-Ritz method and Fourier series. Also, vibrational behavior of single and multi-directional FG annular plates and laminated curved panels was investigated using three-dimensional elasticity theory and generalized differential quadrature method (GDQM)[19-22].

Using the concept of FGM, CNTs can be distributed in certain grading profiles through certain directions to improve the mechanical properties and to reinforce the composite structures. The composites, which are reinforced by CNTs with grading distribution, are called functionally graded carbon nanotube-reinforced composites (FG-CNTRCs). Shen [23] suggested that the interfacial bonding strength can be improved with the use of a graded distribution of CNTs in the matrix. He investigated postbuckling of functionally graded nanocomposite cylindrical shells reinforced by CNTs subjected to axial com-

pression in a thermal environment, and showed that the linear functionally graded reinforcements can increase the buckling load. He estimated mechanical properties with a micro-mechanical model in volume fraction form with CNT efficiency parameters. Mehrabadi et al. [24] discussed mechanical buckling behavior of FG nanocomposite plates reinforced by SWCNTs based on the first-order shear deformation theory (FSDT) and mindlin plate theory. However, the rule of mixture is not applicable when straight CNTs are oriented randomly in the matrix. In these cases the Mori-Tanaka approach [25] is one of the best known analytical approaches to accurately determine the effective material constants of composite materials. Yas and Heshmati [26] used the Mori-Tanaka approach to study the vibrational properties of FG-nanocomposite beams reinforced by randomly oriented straight CNTs under the action of moving load. Sobhani Aragh et al. [27] presented vibrational behavior of continuously graded CNT-reinforced cylindrical panels based on the Eshelby-Mori-Tanaka approach. They used the 2D GDQM to discretize the governing equations and to implement the boundary conditions. Pourasghar et al. [28] and Moradi-Dastjerdi et al. [29] performed a free vibration analysis of FG nanocomposite cylinders reinforced by randomly oriented straight and locally aggregated CNTs, based on both three-dimensional theory of elasticity, and mesh-free methods. Both teams estimated material properties of FG- CNTRCs with the Eshelby-Mori-Tanaka approach. Finally, vibrational behavior of single and multi-directional nanocomposite FG-CNTRC thick plates, sandwich curved panels and annular plates resting on a Pasternak elastic foundation, were investigated using three-dimensional elasticity theory and GDQM [30-34].

Since FSDT violates the equilibrium conditions on the top and bottom surfaces of the plate, a shear correction factor is required to compensate for the error because of a constant shear strain assumption throughout the thickness. The shear correction factor not only depends on the material and its geometric properties, but also on its loading and boundary conditions. Although the FSDT provides a sufficiently accurate description of response for thin to moderately thick plates, it is not convenient to use because of the difficulty in determining the correct value of the shear correction factor. To avoid the use of a shear correction factor, many refined shear deformation plate theories (RSDTs) have been developed including the sinusoidal shear deformation plate theory (SSDT) [35-36], RSDT [37-38], and hyperbolic shear deformation plate theory (HSDT) [39-41]. RSDT is based on an assumption that the in-plane and transverse displacements consist of bending and shear components in which the

bending components do not contribute toward shear forces and, likewise, the shear components do not contribute toward bending moments. The motion equation can be derived from Hamilton's energy principle and Navier's method solves this equation. Moradi-Dastjerdi et al. [42] used an RSDT with only four independent unknowns, and presented the free vibration analysis of sandwich plates with FG randomly oriented CNTRC face sheets resting on an elastic foundation. Khorshidi et al. [43-44] used nonlocal elasticity theory based on exponential shear deformation theory, for free vibration and buckling analyses of the FG rectangular nanoplates. They also used refined trigonometric shear deformation plate theory to study the out-of-plane vibration of the rectangular isotropic plates with different boundary conditions [45].

Although several studies of the free vibration or buckling of FG and FG nanocomposite plates have been carried out based on a variety of plate theories, no studies can be found applying these analyses to aggregated CNT reinforced plates. In this study, the RSDT is developed to investigate the free vibration and buckling analyses of simply supported functionally graded nanocomposite plates reinforced by aggregated single-walled carbon nanotubes (SWCNTs). The applied nanocomposite is assumed a mixture of CNTs (randomly oriented and locally aggregated into some clusters) that are embedded in a polymer. The material properties of the nanocomposite plates are assumed to vary along the thickness of plate and estimated through the Mori-Tanaka method because of its simplicity and accuracy even at a high volume fraction of inclusions. Effects on the natural frequency and critical buckling load of the FG-CNTRC plates by CNT volume fraction, CNT distribution, CNT cluster distribution, and geometric dimensions of the plate are investigated. Effects of loading conditions on the critical buckling load are also examined.

2. Material Properties in FG-CNTRC Reinforced Composite

Consider a CNTRC is made from a mixture of SWCNT (that randomly oriented and locally aggregated into some clusters) and matrix which is assumed to be isotropic. Many studies have been published each with a different focus on mechanical properties of polymer nanotube composites. However, the common theme has been enhancement of Young's modulus. In this section, the effective mechanical properties of the CNT reinforced composite that straight CNTs are oriented randomly, or locally aggregated in to some clusters, are obtained based on the Eshelby-Mori-Tanaka approach. The resulting effective properties for these CNT reinforced composites are isotropic, despite the CNTs being transversely isotropic.

2.1 Composites reinforced with randomly oriented, straight CNTs

In this section, the effective mechanical properties of composites with randomly oriented nonclustered CNTs (as shown in Fig. 1) are studied. The orientation of a straight CNT is characterized by two Euler angles α and β , as shown in Fig. 1. When CNTs are completely randomly oriented in the matrix, the composite is isotropic, and its bulk modulus K and shear modulus G are derived as [46]:

$$K = K_m + \frac{f_r(\delta_r - 3K_m\alpha_r)}{3(f_m + f_r\alpha_r)} \quad (1)$$

$$G = G_m + \frac{f_r(\eta_r - 2G_m\beta_r)}{2(f_m + f_r\beta_r)}$$

where subscripts m and r are referred to matrix and CNT respectively, f is volume fraction and also,

$$\alpha_r = \frac{3(K_m + G_m) + k_r - l_r}{3(G_m + k_r)} \quad (2)$$

$$\delta_r = \frac{1}{3} \left[n_r + 2l_r + \frac{(2k_r + l_r)(3K_m + 2G_m - l_r)}{G_m + k_r} \right] \quad (3)$$

$$\beta_r = \frac{1}{5} \left\{ \frac{4G_m + 2k_r + l_r}{3(G_m + k_r)} + \frac{4G_m}{G_m + p_r} + \frac{2[G_m(3K_m + G_m) + G_m(3K_m + 7G_m)]}{G_m(3K_m + G_m) + m_r(3K_m + 7G_m)} \right\} \quad (4)$$

$$\eta_r = \frac{1}{5} \left[\frac{2}{3}(n_r - l_r) + \frac{8G_m p_r}{G_m + p_r} + \frac{8m_r G_m (3K_m + 4G_m)}{3K_m(m_r + G_m) + G_m(7m_r + G_m)} + \frac{2(k_r - l_r)(2G_m + l_r)}{3(G_m + k_r)} \right] \quad (5)$$

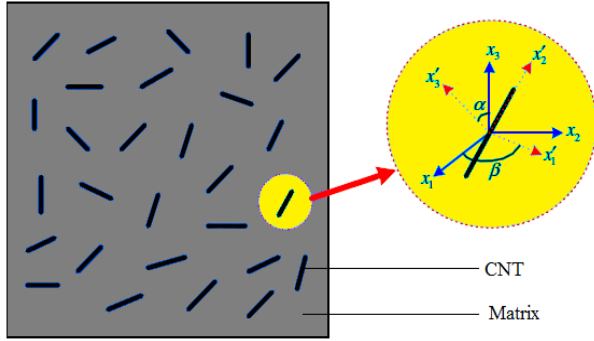


Figure 1. Representative volume element (RVE) with randomly oriented, straight CNTs.

k_r , l_r , m_r , n_r , and p_r are the Hill's elastic moduli for the reinforcing phase (CNTs). As mentioned before, the CNTs are transversely isotropic and have a stiffness matrix given below (Hill's elastic moduli):

$$C_r = \begin{bmatrix} n_r & l_r & l_r & 0 & 0 & 0 \\ l_r & k_r + m_r & k_r - m_r & 0 & 0 & 0 \\ l_r & k_r - m_r & k_r + m_r & 0 & 0 & 0 \\ 0 & 0 & 0 & p_r & 0 & 0 \\ 0 & 0 & 0 & 0 & m_r & 0 \\ 0 & 0 & 0 & 0 & 0 & p_r \end{bmatrix} \quad (6)$$

$$C_r = \begin{bmatrix} \frac{1}{E_L} & -\frac{\nu_{TL}}{E_T} & -\frac{\nu_{ZL}}{E_Z} & 0 & 0 & 0 \\ -\frac{\nu_{LT}}{E_L} & \frac{1}{E_T} & -\frac{\nu_{ZT}}{E_Z} & 0 & 0 & 0 \\ -\frac{\nu_{LZ}}{E_L} & -\frac{\nu_{TZ}}{E_T} & \frac{1}{E_Z} & 0 & 0 & 0 \\ 0 & 0 & 0 & \frac{1}{G_{TZ}} & 0 & 0 \\ 0 & 0 & 0 & 0 & \frac{1}{G_{ZL}} & 0 \\ 0 & 0 & 0 & 0 & 0 & \frac{1}{G_{LT}} \end{bmatrix}^{-1} \quad (7)$$

where E_L , E_T , E_Z , G_{TZ} , G_{ZL} , G_{LT} , ν_{TZ} , ν_{ZL} and ν_{LT} are material properties of the CNT reinforced composite which can be determined from the inverse of the rule of mixture.

So, the effective Young's modulus E and Poisson's ratio ν of the composite is given by:

$$E = \frac{9KG}{3K + G} \quad (8)$$

$$\nu = \frac{3K - 2G}{6K + 2G} \quad (9)$$

2.2 Effect of CNT aggregation on the properties of the composite

The CNTs were arranged within the matrix to introduce clustering. Because of a large aspect ratio (usually >1000), a low bending rigidity, and Van der Waals forces, CNTs have a tendency to bundle or cluster together making it quite difficult to produce fully-dispersed CNT reinforced composites. The effect of nanotube aggregation on the elastic properties of randomly oriented CNTRCs is presented in

this section. Shi et al. [46] derived a two parameter micromechanics model to determine the effect of nanotube agglomeration on the elastic properties of a randomly oriented CNTRC (Fig. 2). It is assumed that a number of CNTs are uniformly distributed throughout the matrix and that other CNTs appear in cluster form because of aggregation, as shown in Fig. 2. The total volume of the CNTs in the representative volume element (RVE), denoted by V_r , can be divided into the following two parts:

$$V_r = V_r^{cluster} + V_r^m \quad (10)$$

where $V_r^{cluster}$ denotes the volumes of CNTs inside a cluster, and V_r^m is the volume of CNTs in the matrix and outside the clusters. The two parameters used to describe the aggregation are defined as:

$$\mu = \frac{V_{cluster}}{V}, \quad \eta = \frac{V_r^{cluster}}{V_r} \quad 0 \leq \eta, \mu \leq 1 \quad (11)$$

where V is the volume of RVE, $V_{cluster}$ is the volume of clusters in the RVE. μ is the volume fraction of clusters with respect to the total volume V of the RVE, η is the volume ratio of the CNTs inside the clusters over the total CNT inside the RVE. When $\mu = 1$, there is uniform distribution of nanotubes throughout the entire composite without aggregation; with a decreasing μ , the agglomeration degree of CNTs becomes more severe. When $\eta = 1$, all nanotubes are located in the clusters. The case $\eta = \mu$ means that the volume fraction of CNTs inside the clusters is equal to that of CNTs outside the clusters, so all CNTs are located and randomly oriented as in Fig. 1. Thus, we consider the CNT-reinforced composite as a system consisting of spherically shaped clusters in a matrix. We first estimate the effective elastic stiffness of the clusters and the matrix respectively, and then calculate the overall property of the whole composite system. The effective bulk modulus K_{in} and shear modulus G_{in} of the cluster can be calculated with Prylutsky et al. [47]:

$$K_{in} = K_m + \frac{f_r \eta (\delta_r - 3K_m \alpha_r)}{3(\mu - f_r \eta + f_r \eta \alpha_r)} \quad (12)$$

$$G_{in} = G_m + \frac{f_r \eta (\eta_r - 2G_m \beta_r)}{2(\mu - f_r \eta + f_r \eta \beta_r)} \quad (13)$$

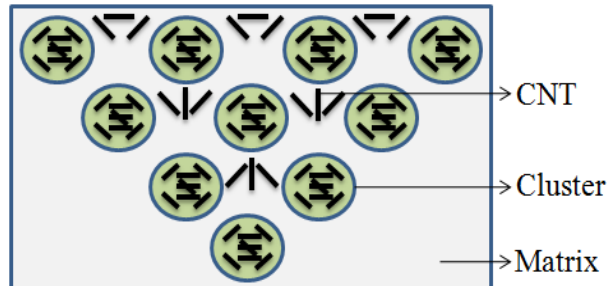


Figure 2. RVE with functionally graded Eshelby cluster model of aggregation of CNTs.

and the effective bulk modulus K_{out} and shear modulus G_{out} of the matrix outside the cluster can be calculated by:

$$K_{out} = K_m + \frac{f_r(1-\eta)(\delta_r - 3K_m\alpha_r)}{3[1-\mu - f_r(1-\eta) + f_r(1-\eta)\alpha_r]} \quad (14)$$

$$G_{out} = G_m + \frac{f_r(1-\eta)(\eta_r - 2G_m\beta_r)}{2[1-\mu - f_r(1-\eta) + f_r(1-\eta)\beta_r]} \quad (15)$$

Finally, the effective bulk modulus K and the effective shear modulus G of the composite are derived from the Mori-Tanaka method as follows:

$$K = K_{out} \left[1 + \frac{\mu \left(\frac{K_{in}}{K_{out}} - 1 \right)}{1 + \alpha(1-\mu) \left(\frac{K_{in}}{K_{out}} - 1 \right)} \right] \quad (16)$$

$$G = G_{out} \left[1 + \frac{\mu \left(\frac{G_{in}}{G_{out}} - 1 \right)}{1 + \beta(1-\mu) \left(\frac{G_{in}}{G_{out}} - 1 \right)} \right] \quad (17)$$

with

$$\nu_{out} = \frac{(3K_{out} - 2G_{out})}{2(3K_{out} + G_{out})} \quad (18)$$

$$\alpha = \frac{(1 + \nu_{out})}{3(1 - \nu_{out})} \quad (19)$$

$$\beta = \frac{2(4 - 5\nu_{out})}{15(1 - \nu_{out})} \quad (20)$$

The effective Young's modulus E and Poisson's ratio ν of the composite can be calculated in the terms of K and G by Eqs. (8) and (9).

3. Refined Plate Theory

Consider a rectangular FG-CNTRC plate with thickness h , and edges parallel to axes x and y , as shown in Fig. 3. The volume fractions of CNTs or f_r , are varied along the thickness of the plate as following:

$$f_r = (f_r^u - f_r^d)(1 + z/h)^p + f_r^d, \quad -h/2 < z < h/2 \quad (21)$$

$$f_m = 1 - f_r \quad (22)$$

Where p ($0 \leq p < \infty$) is the volume fraction exponent and f_r^u and f_r^d are the values of CNT volume fraction in upper ($z = h/2$) and downer surfaces ($z = -h/2$), respectively.

Fig. 4 shows the variation of CNT volume fraction along the thickness of a plate for different values of the volume fraction exponent, p . The effective Young's modulus E and Poisson's ratio ν are obtained from Eqs. (8), (9).

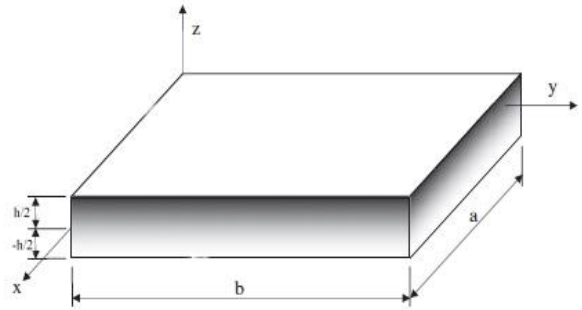


Figure 3. Schematic of the CNTRC plate.

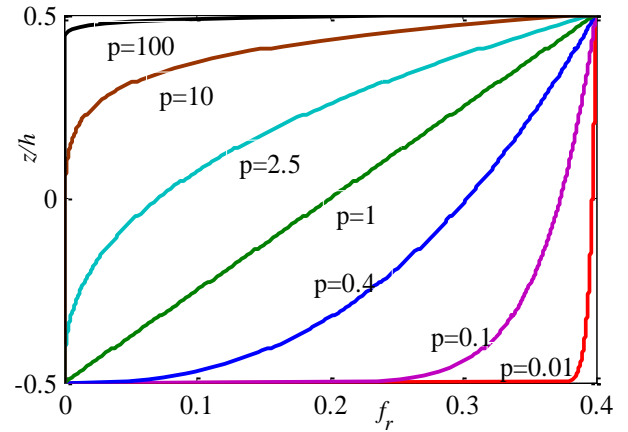


Figure 4. Variation of properties along the thickness of cylinders for different values of p according to Eq. (21).

3.1 Basic assumptions

The assumptions of the present theory are as follows [37]:

a) The displacements are small in comparison with the plate thickness and thus the strains involved are infinitesimal.

b) The transverse displacement W includes two components: bending w_b and shear w_s , and these components are functions of coordinates x, y only.

$$W(x, y, z) = w_b(x, y) + w_s(x, y) \quad (23)$$

c) The transverse normal stress σ_z is negligible in comparison with the in-plane stresses σ_x and σ_y .

d) The displacements U in the x -direction, and V in the y -direction, consist of extension, bending, and shear components.

$$U = u + u_b + u_s, \quad V = v + v_b + v_s \quad (24)$$

The bending components u_b and v_b are assumed to be similar to the displacements given by classical plate theory. Therefore, the expression for u_b and v_b can be given as:

$$u_b = -z \frac{\partial w_b}{\partial x}, \quad v_b = -z \frac{\partial w_b}{\partial y} \quad (25)$$

In conjunction with w_s , the shear components u_s and v_s give rise to the parabolic variations of shear strains γ_{xz} , γ_{yz} and hence to shear stresses τ_{xz} , τ_{yz} across the thickness of the plate in such a way that the shear stresses τ_{xz} , τ_{yz} are zero at the top and

bottom faces of the plate. Consequently, the expression for u_s and v_s can be given as:

$$\begin{aligned} u_s &= \left[\frac{1}{4}z - \frac{5}{3}z \left(\frac{z}{h} \right)^2 \right] \frac{\partial w_s}{\partial x}, \\ v_s &= \left[\frac{1}{4}z - \frac{5}{3}z \left(\frac{z}{h} \right)^2 \right] \frac{\partial w_s}{\partial y} \end{aligned} \quad (26)$$

3.2 Kinematics and constitutive equations

Based on the assumptions made in the preceding section, the displacement field can be obtained [37]

$$\begin{aligned} u(x, y, z) &= u_0(x, y) - z \frac{\partial w_b}{\partial x} - f(z) \frac{\partial w_s}{\partial x} \\ v(x, y, z) &= v_0(x, y) - z \frac{\partial w_b}{\partial y} - f(z) \frac{\partial w_s}{\partial y} \end{aligned} \quad (27)$$

$$w(x, y, z) = w_b(x, y) + w_s(x, y)$$

where

$$f(z) = z \left[\frac{-1}{4} + \frac{5}{3} \left(\frac{z}{h} \right)^2 \right] \quad (28)$$

The strains associated with the displacements in Eq. (27) are:

$$\begin{aligned} \varepsilon_x &= \varepsilon_x^0 + zk_x^b + f(z)k_x^s, \\ \varepsilon_y &= \varepsilon_y^0 + zk_y^b + f(z)k_y^s, \\ \gamma_{xy} &= \gamma_{xy}^0 + zk_{xy}^b + f(z)k_{xy}^s, \\ \gamma_{yz} &= g(z)\gamma_{yz}^s, \gamma_{zx} = g(z)\gamma_{zx}^s \end{aligned} \quad (29)$$

$$\varepsilon_z = 0$$

where

$$\begin{aligned} \varepsilon_x^0 &= \frac{\partial u_0}{\partial x}, k_x^b = -\frac{\partial^2 w_b}{\partial x^2}, k_x^s = -\frac{\partial^2 w_s}{\partial x^2} \\ \varepsilon_y^0 &= \frac{\partial v_0}{\partial y}, k_y^b = -\frac{\partial^2 w_b}{\partial y^2}, k_y^s = -\frac{\partial^2 w_s}{\partial y^2} \\ \gamma_{xy}^0 &= \frac{\partial u_0}{\partial y} + \frac{\partial v_0}{\partial x}, k_{xy}^b = -2 \frac{\partial^2 w_b}{\partial x \partial y}, \\ k_{xy}^s &= -2 \frac{\partial^2 w_s}{\partial x \partial y} \end{aligned} \quad (30)$$

$$\gamma_{yz}^s = \frac{\partial w_s}{\partial y}, \gamma_{zx}^s = \frac{\partial w_s}{\partial x}, g(z) = 1 - \frac{df(z)}{dz}$$

For elastic and isotropic materials, the constitutive relations can be written as:

$$\begin{aligned} \begin{Bmatrix} \sigma_x \\ \sigma_y \\ \tau_{xy} \end{Bmatrix} &= \begin{bmatrix} Q_{11} & Q_{12} & 0 \\ Q_{12} & Q_{22} & 0 \\ 0 & 0 & Q_{66} \end{bmatrix} \begin{Bmatrix} \varepsilon_x \\ \varepsilon_y \\ \gamma_{xy} \end{Bmatrix} \\ \begin{Bmatrix} \tau_{yz} \\ \tau_{zx} \end{Bmatrix} &= \begin{bmatrix} Q_{44} & 0 \\ 0 & Q_{55} \end{bmatrix} \begin{Bmatrix} \gamma_{yz} \\ \gamma_{zx} \end{Bmatrix} \end{aligned} \quad (31)$$

where $(\sigma_x, \sigma_y, \tau_{xy}, \tau_{yz}, \tau_{zx})$ and $(\varepsilon_x, \varepsilon_y, \gamma_{xy}, \gamma_{yz}, \gamma_{zx})$ are the stress and strain components, respectively.

Using the material properties defined in Eq. (21), stiffness coefficients, Q_{ij} , can be expressed as:

$$\begin{aligned} Q_{11} = Q_{22} &= \frac{E(z)}{1-\nu^2}, \quad Q_{12} = \frac{\nu E(z)}{1-\nu^2}, \\ Q_{66} = Q_{44} = Q_{55} &= \frac{E(z)}{2(1+\nu)} \end{aligned} \quad (32)$$

3.3 Governing equations

Using Hamilton's energy principle the motion equation of the isotropic plate is derived:

$$\delta \int_{t_1}^{t_2} (U + V - K) dt = 0 \quad (33)$$

where U is the strain energy, V work done by applied forces, and K is the kinetic energy of the isotropic plate. Employing the minimum of the total energy principle leads to a general equation of motion and boundary conditions. Taking the variation of the above equation and integrating by parts:

$$\begin{aligned} \int_{t_1}^{t_2} \int_V [\sigma_x \delta \varepsilon_x + \sigma_y \delta \varepsilon_y + \tau_{xy} \delta \gamma_{xy} + \tau_{yz} \delta \gamma_{yz} \\ + \tau_{zx} \delta \gamma_{zx} - \rho(\ddot{u} \delta u + \ddot{v} \delta v + \ddot{w} \delta w)] dv \\ + \int_A (N_x^0 (\delta w_{b,x} + \delta w_{s,x}) + N_y^0 (\delta w_{b,y} \\ + \delta w_{s,y})) dA] dt = 0 \end{aligned} \quad (34)$$

where $\ddot{}$ represents the second derivative with respect to time and also (N_x^0, N_y^0) are in-plane pre-buckling forces.

The equations of motion can be obtained by substitution of Eqs. (27) and (29) into Eq. (34) and by consideration of the following assumptions. The stress resultants N, M, S and the mass moments of inertia are defined by:

$$\begin{bmatrix} N_x & N_y & N_{xy} \\ M_x^b & M_y^b & M_{xy}^b \\ M_x^s & M_y^s & M_{xy}^s \end{bmatrix} = \int_{-\frac{h}{2}}^{\frac{h}{2}} (\sigma_x, \sigma_y, \tau_{xy}) \begin{pmatrix} 1 \\ z \\ f(z) \end{pmatrix} dz \quad (35.a)$$

$$(s_{xz}^s, s_{yz}^s) = \int_{-\frac{h}{2}}^{\frac{h}{2}} (\tau_{xz}, \tau_{yz}) g(z) dz \quad (35.b)$$

$$\begin{aligned} (I_1, I_2, I_3, I_4, I_5, I_6) \\ = \int_{-\frac{h}{2}}^{\frac{h}{2}} \rho(z) (1, z, z^2, f(z), zf(z), (f(z))^2) dz \end{aligned} \quad (35.c)$$

So, the equation of motion can be written as:

$$\delta u_0: N_{x,x} + N_{xy,y} = I_2 \ddot{w}_{b,x} + I_4 \ddot{w}_{s,x} - I_1 \ddot{u}_0 \quad (36.a)$$

$$\delta v_0: N_{y,y} + N_{xy,x} = I_2 \ddot{w}_{b,y} + I_4 \ddot{w}_{s,y} - I_1 \ddot{v}_0 \quad (36.b)$$

$$\begin{aligned} \delta w_b: M_{x,xx}^b + M_{y,yy}^b + 2M_{xy,xy}^b + p(w) \\ = I_3 (\ddot{w}_{b,xx} + \ddot{w}_{b,yy}) + I_5 (\ddot{w}_{s,xx} + \ddot{w}_{s,yy}) \\ - I_2 (\ddot{u}_{0,x} + \ddot{v}_{0,y}) - I_1 (\ddot{w}_b + \ddot{w}_s) \end{aligned} \quad (36.c)$$

$$\begin{aligned} \delta w_s: M_{x,xx}^s + M_{y,yy}^s + 2M_{xy,xy}^s + s_{yz,y}^s \\ + s_{xz,x}^s + p(w) \\ = I_5 (\ddot{w}_{b,xx} + \ddot{w}_{b,yy}) + I_6 (\ddot{w}_{s,xx} + \ddot{w}_{s,yy}) \\ - I_4 (\ddot{u}_{0,x} + \ddot{v}_{0,y}) - I_1 (\ddot{w}_b + \ddot{w}_s) \end{aligned} \quad (36.d)$$

where

$$p(w) = N_x^0 (w_{b,xx} + w_{s,xx}) + N_y^0 (w_{b,yy} + w_{s,yy}) \quad (37)$$

Substituting Eq. (31) into Eq. (35) and integrating through the thickness of the plate, the stress resultants are given as:

$$\begin{Bmatrix} N \\ M^b \\ M^s \end{Bmatrix} = \begin{bmatrix} A & B & B^s \\ B & D & D^s \\ B^s & D^s & H^s \end{bmatrix} \begin{Bmatrix} \varepsilon \\ k^b \\ k^s \end{Bmatrix}, \quad S = A^s \gamma \quad (38)$$

where

$$\begin{aligned} N = \{N_x, N_y, N_{xy}\}^T, M^b = \{M_x^b, M_y^b, M_{xy}^b\}^T, \\ M^s = \{M_x^s, M_y^s, M_{xy}^s\}^T \end{aligned} \quad (39)$$

$$\epsilon = \{\epsilon_x^0, \epsilon_y^0, \gamma_{xy}^0\}^T, k^b = \{k_x^b, k_y^b, k_{xy}^b\}^T, \quad (40)$$

$$k^s = \{k_x^s, k_y^s, k_{xy}^s\}^T \quad (41)$$

$$S = \{S_{xz}^s, S_{yz}^s\}^T, \gamma = \{\gamma_{xz}, \gamma_{yz}\}^T$$

$$A = \begin{bmatrix} A_{11} & A_{12} & 0 \\ A_{12} & A_{22} & 0 \\ 0 & 0 & A_{66} \end{bmatrix}, \quad (42)$$

$$B = \begin{bmatrix} B_{11} & B_{12} & 0 \\ B_{12} & B_{22} & 0 \\ 0 & 0 & B_{66} \end{bmatrix}, D = \begin{bmatrix} D_{11} & D_{12} & 0 \\ D_{12} & D_{22} & 0 \\ 0 & 0 & D_{66} \end{bmatrix}$$

$$B^s = \begin{bmatrix} B_{11}^s & B_{12}^s & 0 \\ B_{12}^s & B_{22}^s & 0 \\ 0 & 0 & B_{66}^s \end{bmatrix}, D^s = \begin{bmatrix} D_{11}^s & D_{12}^s & 0 \\ D_{12}^s & D_{22}^s & 0 \\ 0 & 0 & D_{66}^s \end{bmatrix},$$

$$H^s = \begin{bmatrix} H_{11}^s & H_{12}^s & 0 \\ H_{12}^s & H_{22}^s & 0 \\ 0 & 0 & H_{66}^s \end{bmatrix}, A^s = \begin{bmatrix} A_{44}^s & 0 \\ 0 & A_{55}^s \end{bmatrix}$$

and stiffness components are given as:

$$\{A_{ij}, B_{ij}, D_{ij}, B_{ij}^s, D_{ij}^s, H_{ij}^s\} = \int_{-\frac{h}{2}}^{\frac{h}{2}} \{1, z, z^2, f(z), zf(z), (f(z))^2\} Q_{ij} dz \quad (43)$$

$$A_{44}^s = A_{55}^s = \int_{-\frac{h}{2}}^{\frac{h}{2}} \frac{E(z)}{2(1+\nu)} [g(z)]^2 dz$$

3.4 Navier's solution for simply supported rectangular plates

Rectangular plates are generally classified in accordance with the type of support used. The analytical solutions of Eq. (36) for simply supported FG-CNTRC plates are used here. The following boundary conditions are imposed at the side edges [37]:

$$\begin{aligned} v_0(0, y) = w_b(0, y) = w_s(0, y) = \frac{\partial w_b}{\partial y}(0, y) \\ = \frac{\partial w_s}{\partial y}(0, y) = 0 \\ v_0(a, y) = w_b(a, y) = w_s(a, y) = \frac{\partial w_b}{\partial y}(a, y) \\ = \frac{\partial w_s}{\partial y}(a, y) = 0 \\ u_0(x, 0) = w_b(x, 0) = w_s(x, 0) = \frac{\partial w_b}{\partial x}(x, 0) \\ = \frac{\partial w_s}{\partial x}(x, 0) = 0 \\ u_0(x, b) = w_b(x, b) = w_s(x, b) = \frac{\partial w_b}{\partial x}(x, b) \\ = \frac{\partial w_s}{\partial x}(x, b) = 0 \end{aligned} \quad (44)$$

$$\begin{aligned} N_x(0, y) = M_x^b(0, y) = M_x^s(0, y) = N_x(a, y) \\ = M_x^b(a, y) = M_x^s(a, y) = 0 \\ N_x(x, 0) = M_x^b(x, 0) = M_x^s(x, 0) = N_x(x, b) \\ = M_x^b(x, b) = M_x^s(x, b) = 0 \end{aligned}$$

The displacement functions that satisfy the equations of boundary conditions (Eq. (44)) are selected as the following Fourier series:

$$\begin{pmatrix} u_0 \\ v_0 \\ w_b \\ w_s \end{pmatrix} = \sum_{m=1}^{\infty} \sum_{n=1}^{\infty} \begin{pmatrix} u_{mn} \cos(\lambda x) \sin(\mu y) e^{i\omega t} \\ v_{mn} \sin(\lambda x) \cos(\mu y) e^{i\omega t} \\ w_{bmn} \sin(\lambda x) \sin(\mu y) e^{i\omega t} \\ w_{smn} \sin(\lambda x) \sin(\mu y) e^{i\omega t} \end{pmatrix} \quad (45)$$

where u_{mn}, v_{mn}, w_{bmn} and w_{smn} are the arbitrary parameters to be determined, ω is the eigen frequency associated with $(m,n)^{th}$ eigen mode, $\lambda = m\pi/a$ and $\mu = n\pi/b$. Substituting Eq. (45) into equations of motion (Eq. (36)) we get the below eigenvalue equations for any fixed value of m and n :

$$([k] - \omega^2[M])\{\Delta\} = 0 \quad (46)$$

and the elements of the coefficient matrix k and M are given in Appendix A. To avoid trivial solution of equation (46), the following equations should be solved:

$$|[k] - \omega^2[M]| = 0 \quad (47)$$

or, with pre-multiplying Eq. (36) by $[M]^{-1}$, becomes:

$$|[M]^{-1}[k] - \omega^2[I]| = 0 \quad (48)$$

the natural frequencies (ω) can be derived by solving this equation.

For stability problems, the natural frequency vanishes and the obtained equations allow derivation of results that concern the buckling of a plate subjected to a system of uniform in-plane compressive loads N_x^0 and N_y^0 . Assuming that there is a given ratio between these forces such that $N_x^0 = -N_0$ and $N_y^0 = -\gamma N_0; \gamma = N_y^0/N_x^0$, we get:

$$([k] - N_0[N])\{\Delta\} = 0 \quad (49)$$

where

$$\{\Delta\} = \begin{pmatrix} u_{mn} \\ v_{mn} \\ w_{bmn} \\ w_{smn} \end{pmatrix}, N = \begin{bmatrix} a_{11} & a_{12} & a_{13} & a_{14} \\ a_{12} & a_{22} & a_{23} & a_{24} \\ a_{13} & a_{23} & a_{33} & a_{34} \\ a_{14} & a_{24} & a_{34} & a_{44} \end{bmatrix}, \quad (50)$$

$$M = \begin{bmatrix} m_{11} & 0 & m_{13} & m_{14} \\ 0 & m_{22} & m_{23} & m_{24} \\ m_{13} & m_{23} & m_{33} & m_{34} \\ m_{14} & m_{24} & m_{34} & m_{44} \end{bmatrix}$$

$$N_0 = \begin{bmatrix} 0 & 0 & 0 & 0 \\ 0 & 0 & 0 & 0 \\ 0 & 0 & k & k \\ 0 & 0 & k & k \end{bmatrix}, k = -N_0(\lambda^2 + \gamma\mu^2) \quad (51)$$

4. Results and Discussions

In this section, first the accuracies of applied methods are examined in the calculations of the nanocomposite modulus, free vibration, and buckling, by comparing obtained results with reported corresponding results in the literatures. Second, the effects of plate dimensions, CNT volume fraction, orientation, aggregation, and their variation patterns are investigated regarding the frequency and critical buckling load parameter of FG-CNTRC plates.

4.1 Validation of models

First, the Mori-Tanaka approach that is applied for calculation of the nanocomposite modulus is examined. As defined before, the parameters μ and η are indicators of the volume fractions of clusters, and CNTs in the clusters, respectively. Fig. 5 shows Young's modulus of a CNT-reinforced composite for various value of μ when $\eta=1$ that is compared with the experimental data (by Odegard et al. [48]). This figure shows that at full dispersion of the randomly oriented CNTs, $\mu=1$, Young's modulus has the biggest values. Young's modulus was decreased by increasing the CNTs aggregation (decreasing of the μ) or decreasing the CNTs volume fraction. Also, it can be seen that the aggregation state of $\eta=1$ and $\mu=0.4$ has nearly the same Young's modulus as the experimental data. These results are in agreement with an argument proposed by Barai and Weng [49].

In the following simulations, CNTRC plates are considered made of Poly (methyl- methacrylate, referred as PMMA) as matrix, with CNT as fibers. PMMA is an isotropic material with $E^m = 2.5 GPa$, $\rho^m = 1150 Kg/m^3$ and $\nu^m = 0.34$. The (10, 10) SWCNTs are selected as reinforcements. The adopted material properties for SWCNT are:

$$E_1^{CN} = 5.6466, \quad E_2^{CN} = 7.0800, \quad G_{12}^{CN} = 1.9445TPa, \\ \rho^{CN} = 1400 Kg/m^3 \text{ and } \nu^{CN} = 0.175 \text{ [23].}$$

In this state the effects of distributions and orientations of the CNTs on the Young's modulus of a CNTRC are examined. Fig. 6 shows Young's modulus of alignment, randomly oriented and locally aggregated CNTRCs for various values of volume fraction of the CNTs. This figure shows that alignment orientation of CNTs estimates very high values for effective Young's modulus despite Fig. 5 showing the experimental data has the same values with $\mu=0.4$ and $\eta=1$. Also it can be seen that randomly oriented or fully dispersed, $\mu=\eta=1$, nanotubes have more stiffness than other aggregated states, $\mu=0.4, 0.7, 0.9$. After verification of the Mori-Tanaka approach, free vibration analysis is performed. First normalized frequency parameters (Ω_{11}) of isotropic FGM plates are presented for various values of volume fraction exponent, p , and ratio of length to thickness, a/h , in Table 1. The normalized natural frequency is then defined as:

$$\Omega_{mn} = \omega_{mn} a^2 \sqrt{\rho_m h / D_m} \tag{51}$$

where

$$D_m = \frac{E_m h^3}{12(1 - \nu^2)} \tag{52}$$

the subscript m is used for metal in the applied FGM plate. The comparisons show that the results agree very well with other available solutions.

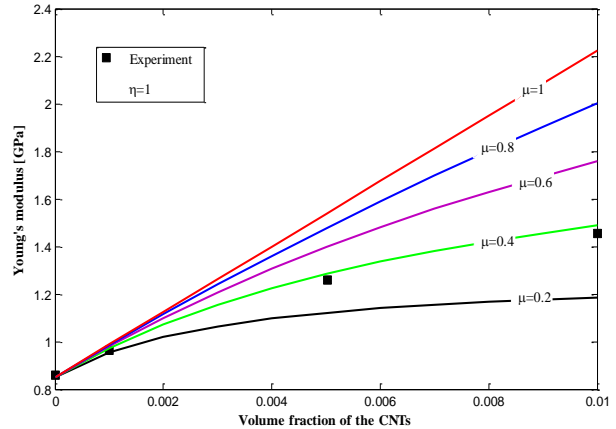


Figure 5. Comparison of the Young's modulus of CNT-reinforced composite at different degree of aggregation with the experimental data from Odegard et al. [48].

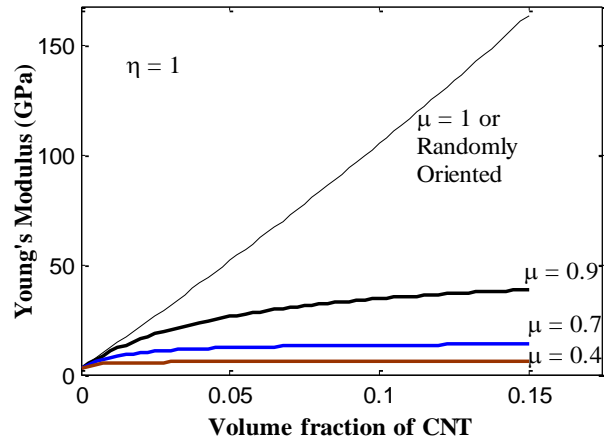


Figure 6. Comparison of the Young's modulus of CNTRC at different degree of aggregation with the randomly oriented and aligned CNTs.

Table 1. Comparison of the first frequency parameters of square isotropic FGM plates.

| a/h | Theory | $p=0$ | $p=1$ | $p=4$ | $p=10$ |
|-------|---------|---------|---------|---------|---------|
| 2 | [50] | 0.9400 | 0.7477 | 0.5997 | 0.5460 |
| | [41] | 0.9300 | 0.7725 | 0.6244 | 0.5573 |
| | Present | 0.9304 | 0.7360 | 0.5928 | 0.5417 |
| 5 | [50] | 0.2121 | 0.1640 | 0.1383 | 0.1306 |
| | [41] | 0.2113 | 0.1740 | 0.1520 | 0.1369 |
| | Present | 0.2113 | 0.1631 | 0.1378 | 0.1301 |
| 10 | [50] | 0.05777 | 0.04427 | 0.03811 | 0.03642 |
| | [41] | 0.05770 | 0.04718 | 0.04210 | 0.03832 |
| | Present | 0.05769 | 0.04419 | 0.03807 | 0.03637 |

Finally, a comparison is carried out for buckling analysis of a simply supported FGM plate with $a/b=1$, $a/h=10$ and the ratio of transverse load to axial load of, $\gamma = N_y/N_x = 0$ (uniaxial compressive pressure). Critical buckling load parameter is defined as $\bar{N} = N_{cr} a^2 / E_m h^3$ and listed in Table 2 for the first mode of FGM plates. These values are compared with results of Bodaghi and Saidi [51] and Thai and Choi [52]. The results agree well with previous results for various values of p .

Table 2. Comparison of the critical buckling load parameters of square isotropic FGM plates with $a/h=10$.

| Theory | $p=0$ | $p=1$ | $p=2$ |
|---------|----------|---------|---------|
| [51] | 1437.361 | 702.304 | 534.441 |
| [52] | 1437.389 | 702.251 | 534.835 |
| present | 1437.390 | 702.251 | 534.837 |

4.2 Free vibration analysis of CNTRC plates

First, simply supported FG-CNTRC square plates are considered. In these plates the volume fraction of randomly oriented CNT, f_r , varies from zero to 0.4 according to Eq. (21) along the thickness of the plate. Fig. 7 shows the first natural frequency parameters, Ω_{11} , that are calculated by the following equation based on the mechanical properties of CNT for various values of p and b/h .

$$\Omega = \omega \frac{b^2}{h} \sqrt{\rho^{CNT} / E_2^{CNT}} \tag{53}$$

This figure shows that by increasing the ratio of width to thickness plates, b/h , or decreasing the volume fraction exponent, p , gives an increase Ω_{11} . Also, Table 3 lists various modes of frequency parameters, $\Omega_{11}, \Omega_{12}, \Omega_{22}, \Omega_{13}$, for the same plate with $a/h=10$. This table shows that UD-CNTRC plates have more values of frequency parameters than FG plates and shows that Ω_{11} and Ω_{13} have the lowest

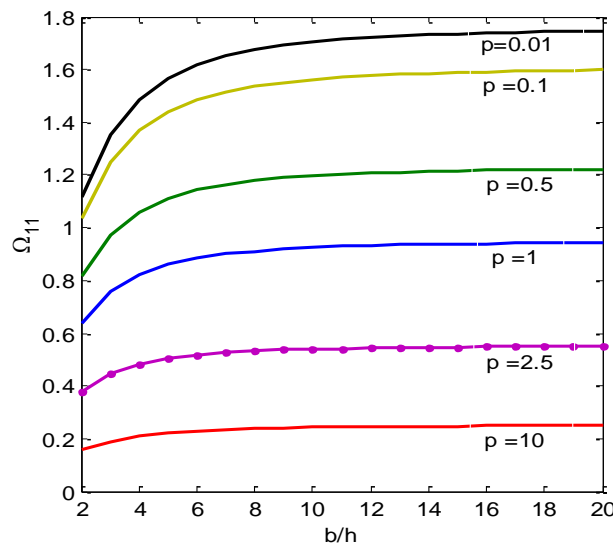


Figure 7. First frequency parameters versus b/h for FG-CNTRC square plates with fully dispersed CNT and $f_r=0-0.4$.

and the highest values of frequency parameters, respectively.

Consider simply supported FG-CNTRC square plates with randomly or aggregated CNT, $a/h=10$ and $f_r = 0 \rightarrow 0.4$. Table 4 shows the first natural frequency parameters of these plates. This table shows that randomly oriented and state of $\mu=\eta=1$, have the highest frequency values and closest values with their material properties. Also, it can be concluded that the parameter of η has more effect than μ on the frequency, and states that are near to fully-dispersed have more frequency values. Fig. 8 illustrates variation of Ω_{11} versus μ for various values of η in UD-CNTRC square plate with $a/h=10$ and $f_r = 0.4$. Frequency parameters increase as μ increases or especially as η decreases. This behavior was seen for mechanical properties of the nanocomposites as well [29]. Fig. 9 shows the first natural frequency of the same plates with $\eta=1$ and various values of μ and a/h . This figure shows that frequency parameters are increased by increasing μ or decreasing the ratio of length to thickness, a/h . As another example, consider FG-CNTRC square plates with $a/h=10$, $f_r = 0 \rightarrow 0.4$ and CNT aggregation state of $\mu=0.5$ and $\eta=1$.

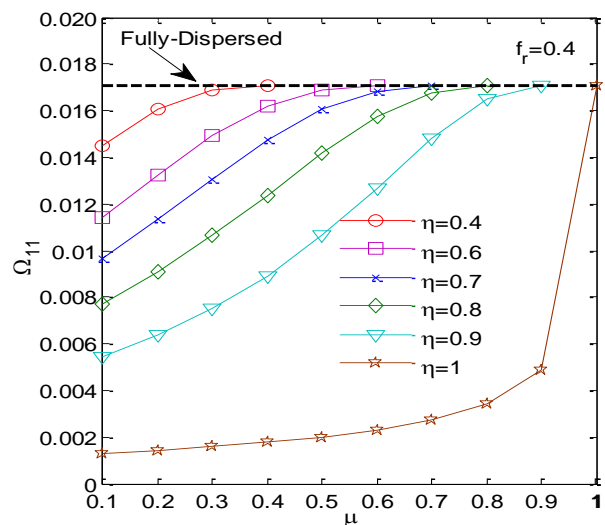


Figure 8. First frequency parameters versus μ for FG-CNTRC square plates with aggregated CNT, $a/h=10$ and $f_r=0.4$.

Table 3. frequency parameters of FG-CNTRC square plates with fully dispersed CNT, $a/h=10$ and $f_r=0-0.4$.

| (m,n) | $p=0.01$ | $p=0.1$ | $p=0.4$ | $p=1$ | $p=2.5$ | $p=10$ | $p=100$ | $f_r=0.2$ |
|---------|----------|---------|---------|--------|---------|--------|---------|-----------|
| (1,1) | 1.6843 | 1.5623 | 1.2708 | 0.9246 | 0.5399 | 0.2425 | 0.1964 | 1.1062 |
| (1,2) | 4.0294 | 3.7427 | 3.0527 | 2.2263 | 1.3013 | 0.5759 | 0.4471 | 2.6450 |
| (2,2) | 6.1980 | 5.7633 | 4.7113 | 3.4431 | 2.0145 | 0.8815 | 0.6628 | 4.0666 |
| (1,3) | 7.5622 | 7.0364 | 5.7597 | 4.2146 | 2.4674 | 1.0730 | 0.7929 | 4.9605 |

Table 4. frequency parameters of FG-CNTRC square plates with $a/h=10$ and $f_r=0-0.4$.

| $(1,1)$ | $p=0.01$ | $p=0.1$ | $p=1$ | $p=10$ | $f_r=0.2$ |
|-------------------------|----------|---------|--------|--------|-----------|
| Randomly | 1.6843 | 1.5623 | 0.9246 | 0.2425 | 1.1062 |
| $\mu = 1, \eta = 1$ | 1.6834 | 1.5616 | 0.9244 | 0.2425 | 1.1059 |
| $\mu = 0.5, \eta = 1$ | 0.2002 | 0.2008 | 0.1986 | 0.1520 | 0.2039 |
| $\mu = 0.7, \eta = 1$ | 0.2731 | 0.2735 | 0.2615 | 0.1685 | 0.2759 |
| $\mu = 0.5, \eta = 0.7$ | 1.5848 | 1.4714 | 0.8755 | 0.2389 | 1.0463 |

Table 5. frequency parameters of FG-CNTRC square plates with $a/h=10, \mu=0.5, \eta=1$ and $f_r=0-0.4$.

| (m,n) | $p=0.01$ | $p=0.1$ | $p=0.4$ | $p=1$ | $p=2.5$ | $p=10$ | $p=100$ | $f_r=0.2$ |
|---------|----------|---------|---------|--------|---------|--------|---------|-----------|
| (1,1) | 0.2002 | 0.2008 | 0.2016 | 0.1986 | 0.1774 | 0.1520 | 0.1327 | 0.2039 |
| (1,2) | 0.4778 | 0.4790 | 0.4811 | 0.4743 | 0.4225 | 0.3612 | 0.3143 | 0.4863 |
| (2,2) | 0.7332 | 0.7352 | 0.7385 | 0.7285 | 0.6559 | 0.5528 | 0.4796 | 0.7463 |
| (1,3) | 0.8935 | 0.8959 | 0.9000 | 0.8882 | 0.8013 | 0.6725 | 0.5826 | 0.9094 |

Table 5 shows various modes of frequency parameters, $\Omega_{11}, \Omega_{12}, \Omega_{22}, \Omega_{13}$, for various values of p . By comparing results of Table 5 and those of Table 3, it can be concluded that aggregation of CNTs sharply decreases frequency parameters in all modes.

In all of the above FG-CNTRC plates, volume fraction of CNT was changed but FG-CNTRC plates can also be made by changing of the volume fraction of clusters. Consider CNTRC square plates with $a/h=10, f_r=0.2$ and $\eta=1$. Volume fraction of clusters of CNTs, μ , varies from zero to 0.4 according to Eq.

(21) along the thickness of plate. Table 6 shows various modes of frequency parameters, $\Omega_{11}, \Omega_{12}, \Omega_{22}, \Omega_{13}$, for various values of volume fraction exponent of clusters, p . This table shows that increasing p decreases frequency parameters in all modes. Fig. 10 illustrates Ω_{11} versus η for distributions of clusters in the CNTRC square plates with $a/h=10$ and $f_r=0.4$. Fig. 10 shows these UD and FG plates have similar values of Ω_{11} for big values of η . Finally, consider a UD-CNTRC square plate with $a/h=10, f_r=0.2, \eta=1$ and $\mu=0.5$. Fig. 11 shows mode shapes of the plate at mode numbers of (1,1), (2,1), (1,2) and (3,1).

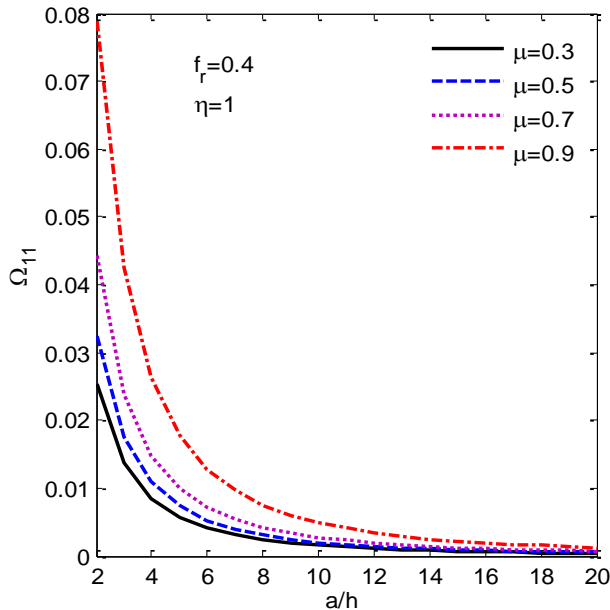


Figure 9. First frequency parameters versus a/h for UD-CNTRC square plates with aggregated CNT and $f_r=0.4$.

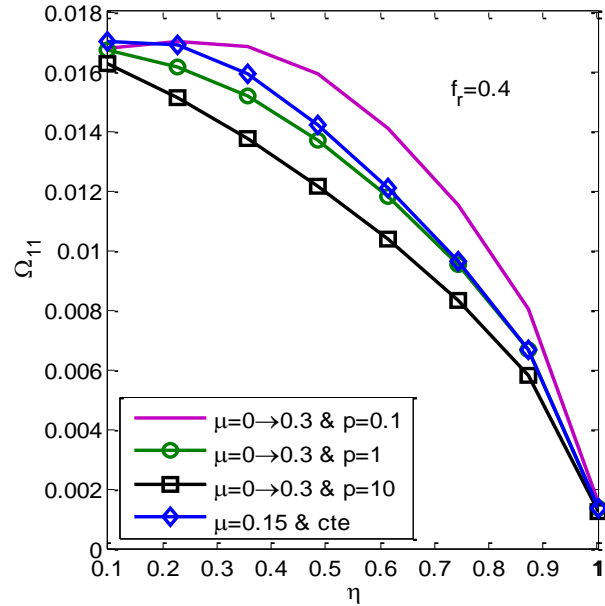


Figure 10. First frequency parameters versus η for UD-CNTRC square plates with aggregated CNT, $a/h=10$ and $f_r=0.4$.

Table 6. frequency parameters of UD-CNTRC square plates with aggregated CNT, $a/h=10, f_r=0.2, \eta=1$ and $\mu=0-0.4$.

| (m,n) | $p=0.01$ | $p=0.1$ | $p=0.4$ | $p=1$ | $p=2.5$ | $p=10$ | $p=100$ | $f_r=0.2$ |
|---------|----------|---------|---------|--------|---------|--------|---------|-----------|
| (1,1) | 0.1791 | 0.1714 | 0.1569 | 0.1455 | 0.1376 | 0.1290 | 0.1203 | 0.1453 |
| (1,2) | 0.4271 | 0.4091 | 0.3746 | 0.3468 | 0.3268 | 0.3058 | 0.2863 | 0.3462 |
| (2,2) | 0.6554 | 0.6281 | 0.5753 | 0.5318 | 0.4995 | 0.4668 | 0.4385 | 0.5309 |
| (1,3) | 0.7986 | 0.7655 | 0.7013 | 0.6478 | 0.6073 | 0.5672 | 0.5336 | 0.6466 |

4.3 Buckling analysis of CNTRC plates

In this section, buckling of FG-CNTRC plates is investigated. First, consider fully dispersed CNT reinforced nanocomposite plates under uniaxial compressive pressure ($\gamma = 0$) with CNT volume fraction of, $f_r=0 \rightarrow 0.4$. The critical buckling load parameters of these plates are listed in Table 7 for various values of plate dimensions (a/b and a/h) and volume fraction exponent (p). The results show that critical buckling load parameter is increased by increasing

the ratios of a/b and a/h or decreasing p . When increasing the aspect ratio of the plates (a/b), they show the behavior of simply supported beams. Thus, the critical buckling load is increased by increasing the ratio of a/b . Also, by considering the definition of critical buckling load parameter, decreasing the plate thickness h , increases critical buckling load parameter. It was observed that in some cases, critical buckling happened at modes of (2, 1), (3, 1) or (4, 1).

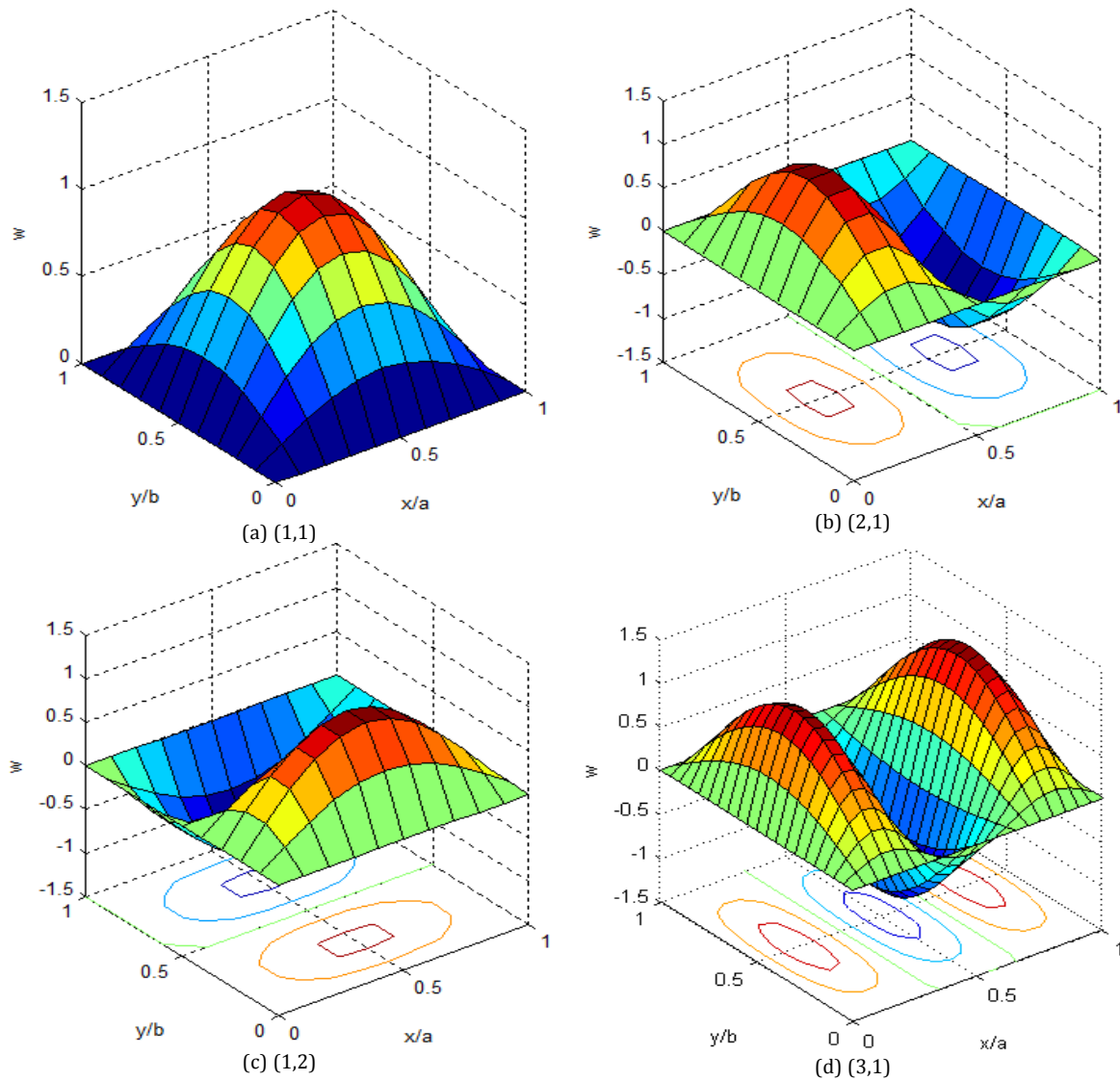


Figure 11. The mode shapes of UD-CNTRC square plates with $\mu=0.5$, $\eta=1$, $a/h=10$ and $f_r=0.2$.

Second, buckling of FG-CNTRC square plates under uniaxial compressive pressure ($\gamma = 0$) with $a/h=10$, $f_r=0 \rightarrow 0.4$ is investigated. Table 8 shows the critical buckling load parameters of the plates for various states of CNT distributions and various values of p . States of $\mu=\eta=1$ and fully dispersion have the biggest and closest buckling parameters, especially at $p=10$. Also, the results reveal that the critical buckling load of the plates has a higher value when distribution of the CNT in polymer is better, as the stiffness of CNTRC plates is larger when CNT distribution is better.

Third, consider FG-CNTRC plates as previously, but instead under biaxial compressive pressure ($\gamma = 1$). Critical buckling load parameters of this third model

of plates are shown in Table 9. Comparing the results of Tables of 8 and 9, shows that critical buckling load parameters of the plates under biaxial compressive load are almost half of the corresponding values of the plates under uniaxial compressive load.

Finally, consider UD-CNTRC plates with $f_r=0.2$ and aggregation state of $\mu=0.5$ and $\eta=1$. Table 10 shows critical buckling load parameters of these plates with various plate dimensions (a/b and a/h) and loading parameter (γ). It can be seen that the critical buckling load parameter is increased by increasing ratios of a/b and a/h , whereas it is decreased by increasing the loading parameter.

Table 7. Critical buckling load parameters of FG-CNTRC plates with fully dispersed CNT, $\gamma = 0$, and $f_r = 0-0.4$.

| a/b | a/h | p | | | | | | | |
|-----|-----|------------------------|------------------------|------------------------|-----------------------|-----------------------|----------------------|----------------------|------------------------|
| | | 0.01 | 0.1 | 0.4 | 1 | 2.5 | 10 | 100 | f _r =0.2 |
| 1 | 2 | 294.8462 ^a | 260.8422 ^a | 186.7806 ^a | 113.2799 ^a | 48.7021 ^a | 7.8708 ^a | 1.8977 ^a | 120.7497 ^a |
| | 5 | 642.5812 | 552.7512 | 366.0923 | 195.3273 | 67.9488 | 13.2080 | 6.8846 | 265.7493 |
| | 10 | 736.8569 | 630.0932 | 411.1198 | 214.7617 | 72.5821 | 14.5825 | 9.3568 | 305.4156 |
| | 30 | 770.4270 | 657.4098 | 426.7051 | 221.3030 | 74.0840 | 15.0505 | 10.4791 | 319.5893 |
| | 100 | 774.4428 | 660.6697 | 428.5542 | 222.0729 | 74.2590 | 15.1057 | 10.6243 | 321.2803 |
| 1.5 | 2 | 354.5132 ^b | 314.8943 ^b | 229.1755 ^b | 144.0864 ^b | 66.6355 ^b | 10.8079 ^b | 2.2533 ^b | 145.0786 ^b |
| | 5 | 1153.5330 ^a | 1002.9824 ^a | 683.1757 ^a | 380.1545 ^a | 140.7012 ^a | 25.5806 ^a | 9.6911 ^a | 475.1888 ^a |
| | 10 | 1629.5324 ^a | 1399.5335 ^a | 923.2362 ^a | 489.7820 ^a | 169.0318 ^a | 33.1534 ^a | 18.2061 ^a | 674.3114 ^a |
| | 30 | 1858.4267 ^a | 1586.7252 ^a | 1031.3711 ^a | 535.9525 ^a | 179.8799 ^a | 36.4333 ^a | 24.7930 ^a | 770.7330 ^a |
| | 100 | 1888.6603 ^a | 1611.2839 ^a | 1045.3228 ^a | 541.7741 ^a | 181.2064 ^a | 36.8507 ^a | 25.8629 ^a | 783.5016 ^a |
| 2 | 2 | 396.9993 ^c | 352.7124 ^c | 258.4639 ^c | 166.0574 ^c | 80.3948 ^c | 13.7075 ^c | 2.6459 ^c | 162.5994 ^c |
| | 5 | 1567.6549 ^b | 1374.9253 ^b | 959.1718 ^b | 554.8582 ^b | 218.7951 ^b | 37.4486 ^b | 11.3034 ^b | 643.8058 ^b |
| | 10 | 2570.3249 ^a | 2211.0049 ^a | 1464.3691 ^a | 781.3092 ^a | 271.7952 ^a | 52.8321 ^a | 27.5384 ^a | 1062.9971 ^a |
| | 30 | 3029.9260 ^a | 2587.5585 ^a | 1682.8889 ^a | 875.2117 ^a | 294.0531 ^a | 59.4851 ^a | 40.1106 ^a | 1256.4700 ^a |
| | 100 | 4817.9138 ^c | 4111.0404 ^c | 2668.1722 ^c | 1383.6709 | 463.1451 ^c | 94.1032 ^c | 65.5928 ^c | 1998.5589 ^c |

^aMode for plate is (m,n)=(2,1) ^bMode for plate is (m,n)=(3,1) ^cMode for plate is (m,n)=(4,1)

Table 8. Critical buckling load parameters of FG-CNTRC square plates with a/h=10, $\gamma = 0$, and $f_r = 0-0.4$.

| | p=0.01 | p=0.1 | p=1 | p=10 | f _r =0.2 |
|-------------------------|----------|----------|----------|---------|---------------------|
| Randomly | 736.8569 | 630.0932 | 214.7617 | 14.5825 | 305.4156 |
| $\mu = 1, \eta = 1$ | 666.4453 | 577.1593 | 204.3684 | 14.3893 | 292.8660 |
| $\mu = 0.5, \eta = 1$ | 10.4138 | 10.4014 | 9.8397 | 5.5833 | 10.3722 |
| $\mu = 0.7, \eta = 1$ | 19.3693 | 19.3032 | 17.0656 | 6.8847 | 19.0047 |
| $\mu = 0.5, \eta = 0.7$ | 652.4199 | 558.9323 | 192.5201 | 14.1503 | 273.2313 |

Table 9. Critical buckling load parameters of FG-CNTRC square plates with a/h=10, $\gamma = 1$, and $f_r = 0-0.4$.

| | p=0.01 | p=0.1 | p=1 | p=10 | f _r =0.2 |
|-------------------------|----------|----------|----------|--------|---------------------|
| Randomly | 368.4285 | 315.0466 | 107.3809 | 7.2912 | 152.7078 |
| $\mu = 1, \eta = 1$ | 333.2226 | 288.5797 | 102.1842 | 7.1946 | 146.4330 |
| $\mu = 0.5, \eta = 1$ | 5.2069 | 5.2007 | 4.9199 | 2.7916 | 5.1861 |
| $\mu = 0.7, \eta = 1$ | 9.6846 | 9.6516 | 8.5328 | 3.4423 | 9.5023 |
| $\mu = 0.5, \eta = 0.7$ | 326.2099 | 279.4662 | 96.2600 | 7.0751 | 136.6156 |

Table 10. Critical buckling load parameters of UD-CNTRC plates with $\mu=0.5, \eta=0.7$, and $f_r = 0.2$.

| a/b | a/h | $\gamma = N_y/N_x$ | | | | | | | |
|-----|-----|------------------------|------------------------|-----------------------|-----------------------|----------------------|----------------------|----------------------|----------------------|
| | | 0 | 0.1 | 0.2 | 0.5 | 1 | 2 | 5 | 10 |
| 1 | 2 | 108.2666 ^a | 105.6259 ^a | 103.1110 ^a | 83.7473 | 62.8105 | 41.8736 | 20.9368 | 11.4201 |
| | 5 | 237.8406 | 216.2187 | 198.2005 | 158.5604 | 118.9203 | 79.2802 | 39.6401 | 21.6219 |
| | 10 | 273.2313 | 248.3921 | 227.6927 | 182.1542 | 136.6156 | 91.0771 | 45.5386 | 24.8392 |
| | 30 | 285.8653 | 259.8776 | 238.2211 | 190.5769 | 142.9327 | 95.2884 | 47.6442 | 25.9878 |
| | 100 | 287.3778 | 261.2525 | 239.4815 | 191.5852 | 143.6889 | 95.7926 | 47.8963 | 26.1530 |
| 1.5 | 2 | 130.1103 ^b | 126.9369 ^b | 123.9146 ^b | 111.8032 ^a | 91.6786 ^a | 67.4107 ^a | 37.5732 ^a | 21.6223 ^a |
| | 5 | 425.5896 ^a | 402.9251 ^a | 382.5524 ^a | 266.8472 | 174.4771 | 103.1001 | 46.2898 | 24.1298 |
| | 10 | 603.4322 ^a | 571.2459 | 482.6043 | 329.3064 | 215.3157 | 127.2320 | 57.1246 | 29.7777 |
| | 30 | 689.4420 ^a | 613.9956 | 518.7204 | 353.9504 | 231.4291 | 136.7536 | 61.3996 | 32.0062 |
| | 100 | 700.8266 ^a | 619.2725 | 523.1785 | 356.9924 | 233.4181 | 137.9289 | 61.9273 | 32.2812 |
| 2 | 2 | 145.8203 ^c | 142.2637 ^c | 138.8765 ^c | 126.5728 ^b | 86.6133 | 48.1185 | 20.6222 | 10.5626 |
| | 5 | 576.9331 ^b | 552.3828 ^b | 523.8876 ^a | 394.0031 | 236.4019 | 131.3344 | 56.2862 | 28.8295 |
| | 10 | 951.3625 ^a | 864.8751 ^a | 792.8021 ^a | 529.7794 | 317.8677 | 176.5932 | 75.6828 | 38.7644 |
| | 30 | 1123.9652 ^a | 1021.7872 ^a | 936.6377 ^a | 590.4315 | 354.2589 | 196.8105 | 84.3474 | 43.2023 |
| | 100 | 1147.7093 ^a | 1043.3721 ^a | 956.4245 ^a | 598.2341 | 358.9405 | 199.4114 | 85.4620 | 43.7732 |

^aMode for plate is (m,n)=(2,1) ^bMode for plate is (m,n)=(3,1) ^cMode for plate is (m,n)=(4,1)

5. Conclusions

In this paper the effects of various parameters on the natural frequency and critical buckling load of simply supported FG-CNTRC plates are investigated. The randomly oriented nanotubes were assumed to have aggregated into some clusters and the Mori-Tanaka approach was used to estimate the mechanical properties of nanocomposites. The motion

equation was derived from Hamilton’s energy principle and Navier’s method solved this equation. The following results are obtained from these analyses:

- Fully dispersed and state of $\mu=\eta=1$ for CNT distribution have the biggest and closest frequency values and critical buckling load as their material properties.
- The parameter of η has more effect than μ on the frequency and critical buckling load of the plates.

- The frequency parameter and critical buckling load increase as μ increases or especially as η decreases.
- Aggregation of CNTs sharply decreases frequency parameters and critical buckling loads in all modes.
- With equal CNT volume fraction, UD-CNTRC plates have more values of frequency parameters and critical buckling than FG plates with linear distribution.
- The frequency parameter and critical buckling load parameter are increased by increasing the ratio of a/h or decreasing the volume fraction exponent of CNT and cluster.
- The critical buckling load parameters of the plates under biaxial compressive load are nearly half of the corresponding values of the plates under uniaxial compressive load.
- The critical buckling load is increased by increasing ratios a/b and a/h , whereas it is decreased by increasing the loading parameter.

Appendix

$$\begin{aligned}
 a_{11} &= (A_{11}\lambda^2 + A_{66}\mu^2), \\
 a_{12} &= (A_{12} + A_{66})\mu\lambda, \\
 a_{13} &= -(B_{11}\lambda^2 + \mu^2(B_{12} + 2B_{66}))\lambda, \\
 a_{14} &= -(B_{11}^s\lambda^2 + \mu^2(B_{12}^s + 2B_{66}^s))\lambda, \\
 a_{22} &= (A_{22}\mu^2 + A_{66}\lambda^2), \\
 a_{23} &= -(\lambda^2(B_{12} + 2B_{66}) + B_{22}\mu^2)\mu \\
 a_{24} &= -(\lambda^2(B_{12}^s + 2B_{66}^s) + B_{22}^s\mu^2)\mu, \\
 a_{33} &= (D_{11}\lambda^4 + 2D_{12}\lambda^2\mu^2 + D_{22}\mu^4 + 4D_{66}\lambda^2\mu^2 + k_0 + k_1(\lambda^2 + \mu^2)), \\
 a_{34} &= (D_{11}^s\lambda^4 + 2D_{12}^s\lambda^2\mu^2 + D_{22}^s\mu^4 + 4D_{66}^s\lambda^2\mu^2 + k_0 + k_1(\lambda^2 + \mu^2)), \\
 a_{44} &= (H_{11}^s\lambda^4 + 2H_{12}^s\lambda^2\mu^2 + H_{22}^s\mu^4 + 4H_{66}^s\lambda^2\mu^2 + k_0 + k_1(\lambda^2 + \mu^2) + \mu^2 A_{44}^s + \lambda^2 A_{55}^s), \\
 m_{11} &= m_{22} = m_{44} = -I_1, \quad m_{13} = I_2\lambda, \quad m_{14} = I_4\lambda, \\
 m_{23} &= I_2\mu, \quad m_{24} = I_4\mu, \quad m_{33} = -(I_3(\lambda^2 + \mu^2) + I_1), \\
 m_{34} &= -(I_5(\lambda^2 + \mu^2) + I_1)
 \end{aligned}$$

References

- [1] Esawi AMK, Farag MM, Carbon nanotube reinforced composites: potential and current challenges. *Mate Des*, 2007; 28: 2394-2401.
- [2] Lau AKT, Hui D, The revolutionary creation of new advanced materials-carbon nanotube composites. *Compos Part B*, 2002; 33: 263-277.
- [3] Thostenson ET, Ren Z, Chou TW, Advances in the science and technology of carbon nanotubes and their composites: a review. *Compos Sci Technol*, 2001; 61: 1899-1912.
- [4] Han Y, Elliott J, Molecular dynamics simulations of the elastic properties of polymer/carbon nanotube composites. *Comput Mater Sci*, 2007; 39: 315-323.
- [5] Alian, AR, Kundalwal, SI, Meguid, SA, Multiscale modeling of carbon nanotube epoxy composites, *Polym*, 2015; 70, 149-160.
- [6] Kundalwal, SI, Ray MC, Smart damping of fuzzy fiber reinforced composite plates using 1--3 piezoelectric composites, *J Vib Control*, 2016; 22: 1526-1546.
- [7] Kundalwal, SI, Meguid, SA, Effect of carbon nanotube waviness on active damping of laminated hybrid composite shells, *Acta Mech*, 2015; 226, 2035-2052.
- [8] Ray, MC, Kundalwal, SI, Effect of Carbon Nanotube Waviness on the Load Transfer Characteristics of Short Fuzzy Fiber-Reinforced Composite, *J Nanomech Micromech*, 2013; 4, A4013010.
- [9] Wuite J, Adali S, Deflection and stress behaviour of nanocomposite reinforced beams using a multiscale analysis. *Compos struct*, 2005; 71: 388-396.
- [10] Formica G, Lacarbonara W, Alessi R, Vibrations of carbon nanotube reinforced composites. *J Sound Vib*, 2010; 329: 1875-1889.
- [11] Vodenitcharova T, Zhang LC, Bending and local buckling of a nanocomposite beam reinforced by a single-walled carbon nanotube. *Inter J Solid Struct*, 2006; 43: 3006-3024.
- [12] Reddy JN, Analysis of functionally graded plates. *Int J Numerical Methods Eng*, 2000; 47: 663-684.
- [13] Zenkour AM, A comprehensive analysis of functionally graded sandwich plates. Part 2-buckling and free vibration deflection and stresses. *Inter J Solid Struct*, 2005; 42: 5243-5258.
- [14] Cheng ZQ, Batra RC, Deflection relationships between the homogeneous Kirchhoff plate theory different functionally graded plate theories. *Archive Mech*, 2000; 52: 143-158.
- [15] Cheng ZQ, Batra RC, Exact correspondence between eigenvalues of membranes and functionally graded simply supported polygonal plates. *J Sound Vib*, 2000; 229: 879-895.
- [16] Amabili, M, Karazis, K, Khorshidi, K, Nonlinear vibrations of rectangular laminated composite plates with different boundary conditions, *Inter J Struct Stab Dyn*, 2011; 11, 673-695.
- [17] Khorshidi, K, Farhadi, S, Free vibration analysis of a laminated composite rectangular plate in contact with a bounded fluid, *Compos struct*, 2013; 104, 176-186.
- [18] Khorshidi, K, Bakhsheshy, A, Free vibration analysis of a functionally graded rectangular plate in contact with a bounded fluid, *Acta Mech*, 2015; 226, 3401-3423.

- [19] Tahouneh, V, Naei, MH, Semi-Analytical Solution for Free Vibration Analysis of Thick Laminated Curved Panels with Power-Law Distribution FG Layers and Finite Length Via Two-Dimensional GDQ Method, *J solid mech*, 2016; 8, 334-347.
- [20] Tahouneh, V, Naei, MH, Free vibration and vibrational displacements analysis of thick elastically supported laminated curved panels with power-law distribution functionally graded layers and finite length via 2D GDQ method, *J Sandw Struct Mater*, 2016; 18, 263-293.
- [21] Tahouneh, V, Yas, MH, Tourang, H, Kabirian, M, Semi-analytical solution for three-dimensional vibration of thick continuous grading fiber reinforced (CGFR) annular plates on Pasternak elastic foundations with arbitrary boundary conditions on their circular edges, *Meccanica*, 2013; 48, 1313-1336.
- [22] Tahouneh, V, Yas, MH, Semi-analytical solution for three-dimensional vibration analysis of thick multidirectional functionally graded annular sector plates under various boundary conditions, *J Eng Mech*, 2013, 140, 31-46.
- [23] Shen HS, Postbuckling of nanotube-reinforced composite cylindrical shells in thermal environments, Part I: Axially-loaded shells. *Compos struct*, 2011; 93: 2096-20108.
- [24] Mehrabadi SJ, Sobhani Aragh B, Khoshkharesh V, Taherpour A, Mechanical buckling of nanocomposite rectangular plate reinforced by aligned and straight single-walled carbon nanotubes. *Compos Part B*, 2012; 43: 2031-2040.
- [25] Mori T, Tanaka K, Average stress in matrix and average elastic energy of materials with Misfitting inclusions. *Acta Metallurgica*, 1973; 21: 571-574.
- [26] Yas MH, Heshmati M, Dynamic analysis of functionally graded nanocomposite beams reinforced by randomly oriented carbon nanotube under the action of moving load. *Applied Math Modelling*, 2012; 36: 1371-1394.
- [27] Sobhani Aragh B, Nasrollah Barati AH, Hedayati H, Eshelby-Mori-Tanaka approach for vibrational behavior of continuously graded carbon nanotube-reinforced cylindrical panels. *Compos Part B*, 2012; 43: 1943-1954.
- [28] Pourasghar A, Yas MH, Kamarian S, Local aggregation effect of CNT on the vibrational behavior of four-parameter continuous grading nanotube-reinforced cylindrical panels. *Polymer Compos*, 2013; 34: 707-721.
- [29] Moradi-Dastjerdi R, Pourasghar A, Foroutan M, The effects of carbon nanotube orientation and aggregation on vibrational behavior of functionally graded nanocomposite cylinders by a mesh-free method. *Acta Mech*, 2013; 224: 2817-2832.
- [30] Tahouneh, V, Eskandari-Jam, J, A Semi-analytical Solution for 3-D Dynamic Analysis of Thick Continuously Graded Carbon Nanotube-reinforced Annular Plates Resting on a Two-parameter Elastic Foundation, *Mech Adv compos struct*, 2014; 1, 113-130.
- [31] Tahouneh, V, Yas, MH, Influence of equivalent continuum model based on the Eshelby-Mori-Tanaka scheme on the vibrational response of elastically supported thick continuously graded carbon nanotube-reinforced annular plates, *Polym Compos*, 2014; 35, 1644-1661.
- [32] Tahouneh, V, Naei, MH, The effect of multidirectional nanocomposite materials on the vibrational response of thick shell panels with finite length and rested on two-parameter elastic foundations, *Int J Adv Struct Eng*, 2016; 8, 11-28.
- [33] Tahouneh, V, Using an equivalent continuum model for 3D dynamic analysis of nanocomposite plates, *Steel Compos Struct*, 2016; 20, 623-649.
- [34] Tahouneh, V, Naei, MH, Using Eshelby-Mori-Tanaka scheme for 3D free vibration analysis of sandwich curved panels with functionally graded nanocomposite face sheets and finite length, *Polym Compos*, 2016; DOI: 10.1002/pc.23929.
- [35] AM Zenkour, Generalized shear deformation theory for bending analysis of functionally graded plates. *Applied Math Modelling*, 2006; 30: 67-84.
- [36] Zenkour AM, The refined sinusoidal theory for FGM plates on elastic foundations, *Inter J Mech Sci*, 2009; 51, 869-880.
- [37] Merdaci S, Tounsi A, Houari MS, Mechab I, Hebbali H, Benyoucef S, Two new refined shear displacement models for functionally graded sandwich plates. *Archive Applied Mech*, 2011; 81: 1507-1522.
- [38] Thai HT, Choi DH, A refined plate theory for functionally graded plates resting on elastic foundation. *Compos Sci Technol*, 2011; 71: 1850-1858.
- [39] Akavci SS, Buckling and free vibration analysis of symmetric and antisymmetric laminated composite plates on an elastic foundation. *J Reinf Plast Compos*, 2007; 26: 1907-1919.

- [40] Benyoucef S, Mechab I, Tounsi A, Fekrar A, Ait Atmane H, Adda Bedia EA, Bending of thick functionally graded plates resting on Winkler-Pasternak elastic foundations. *Mech Compos Mater*, 2010; 46: 425-434.
- [41] Moradi-Dastjerdi, R, Payganeh, G, Malek-Mohammadi, H, Free Vibration Analyses of Functionally Graded CNT Reinforced Nanocomposite Sandwich Plates Resting on Elastic Foundation, *J solid mech*, 2015; 7, 158-172
- [42] Khorshid, K, Fallah, A, Buckling analysis of functionally graded rectangular nano-plate based on nonlocal exponential shear deformation theory, *Inter J Mech Sci*, 2016; 113, 94-104.
- [43] Khorshidi, K, Asgari, T, Fallah, A, Free Vibrations Analysis of Functionally Graded Rectangular Nano-plates based on Nonlocal Exponential Shear Deformation Theory, *Mech Adv Compos Struct*, 2015; 2, 79-93.
- [44] Khorshidi, K, Khodadadi, M, Precision Closed-form Solution for Out-of-plane Vibration of Rectangular Plates via Trigonometric Shear Deformation Theory, *Mech Adv Compos Struct*, 2016; 3, 31-43.
- [45] Ait Atmane H, Tounsi A, Mechab I, Adda Bedia EA, Free vibration analysis of functionally graded plates resting on Winkler-Pasternak elastic foundations using a new shear deformation theory. *Inter J Mech Mater Des*, 2010; 6: 113-121.
- [46] Shi DL, Feng XQ, Yonggang YH, Hwang KC, Gao, H, The effect of nanotube waviness and agglomeration on the elastic property of carbon nanotube reinforced composites. *J Eng Mater Technol*, 2004; 126, 250-257.
- [47] Prylutskyi YI, Durov SS, Ogloblya OV, Buzaneva EV, Scharff P, Molecular dynamics simulation of mechanical, vibrational and electronic properties of carbon nanotubes. *Comput Mater Sci*, 2000; 17: 352-355.
- [48] Odegard GM, Gates TS, Wise KE, Park C, Siochi EJ, Constitutive modeling of nanotube-reinforced polymer composites. *Compos Sci Technol*, 2003; 63: 1671-1687.
- [49] Barai P, Weng GJ, A theory of plasticity for carbon nanotube reinforced composite. *Inter J Plast Technol*, 2011; 27: 539-559.
- [50] Matsunaga H, Free vibration and stability of functionally graded plates according to a 2D higher-order deformation theory. *Compos struct*, 2008; 82: 499-512.
- [51] Bodaghi M, Saidi AR, Levy-type solution for buckling analysis of thick functionally graded rectangular plates based on the higher-order shear deformation plate theory. *Appl Math Modelling*, 2010; 34, 3659-3673.
- [52] Thai, HT, Choi, DH, An efficient and simple refined theory for buckling analysis of functionally graded plates. *Appl Math Modelling*, 2012; 36: 1008-1022.